New Frontiers of Metallomics: Elemental and Species-Specific Analysis and Imaging of Single Cells

Javier Jiménez-Lamana, Joanna Szpunar, Ryszard Lobinski

To cite this version:

Javier Jiménez-Lamana, Joanna Szpunar, Ryszard Lobinski. New Frontiers of Metallomics: Elemental and Species-Specific Analysis and Imaging of Single Cells. Arruda M. Metallomics:The Science of Biometals, 1055, Springer International , pp.245 - 270, 2018, 10.1007/978-3-319-90143-5_10 . hal-03133546

HAL Id: hal-03133546
https://hal.science/hal-03133546v1
Submitted on 6 Feb 2021

Chapter 10

New Frontiers of Metallomics: Elemental and Species-Specific Analysis and Imaging of Single Cells

Javier Jiménez-Lamana, Joanna Szpunar, and Ryszard Łobinski

Abstract Single cells represent the basic building units of life, and thus their study is one the most important areas of research. However, classical analysis of biological cells eludes the investigation of cell-to-cell differences to obtain information about the intracellular distribution since it only provides information by averaging over a huge number of cells. For this reason, chemical analysis of single cells is an expanding area of research nowadays. In this context, metallomics research is going down to the single-cell level, where high-resolution high-sensitive analytical techniques are required. In this chapter, we present the latest developments and applications in the fields of single-cell inductively coupled plasma mass spectrometry (SC-ICP-MS), mass cytometry, laser ablation (LA)-ICP-MS, nanoscale secondary ion mass spectrometry (nanoSIMS), and synchrotron X-ray fluorescence microscopy (SXRF) for single-cell analysis. Moreover, the capabilities and limitations of the current analytical techniques to unravel single-cell metabolomics as well as future perspectives in this field will be discussed.

Keywords Single-cell analysis · ICP-MS · Laser ablation · NanoSIMS · X-ray fluorescence · Imaging · Intracellular distribution · Metal content

---

J. Jiménez-Lamana (✉) · J. Szpunar · R. Łobinski
Laboratoire de Chimie Analytique Bio-inorganique et Environnement (LCABIE), UMR 5254-IPREM, CNRS-UPPA, Pau, France
e-mail: j.jimenez-lamana@univ-pau.fr; joanna.szpunar@univ-pau.fr; ryszard.lobinski@univ-pau.fr

M. A. Z. Arruda (ed.), *Metallomics*, Advances in Experimental Medicine and Biology 1055, https://doi.org/10.1007/978-3-319-90143-5_10

Abbreviations

ALOD	Absolute limit of detection
AP-MALDI	Atmospheric pressure matrix-assisted laser desorption ionization
CE	Capillary electrophoresis
cryo-XT	Cryo nanoscale X-ray tomography
CyTOF	Cytometry by time-of-flight
ESI-MS	Electrospray ionization mass spectrometry
fs-LI-O-TOFMS	Femtosecond laser ionization orthogonal time-of-flight mass spectrometry
HECIS	High-efficiency cell introduction system
HPCN	High performance concentric nebulizer
ICP-AES	Inductively coupled plasma atomic emission spectrometry
ICP-MS	Inductively coupled plasma mass spectrometry
ICP-SFMS	Inductively coupled plasma sector field mass spectrometry
ICP-TOFMS	Inductively coupled plasma time-of-flight mass spectrometry
LADE	Liquid-assisted droplet ejection
LA-ICP-MS	Laser ablation inductively coupled plasma mass spectrometry
LB-HPCN	Large-bore high performance concentric nebulizer
MALDI	Matrix-assisted laser desorption ionization
µDG	Micro-droplet generator
M-DIS	Micro-droplet injection system
µFI	Micro-flow Injection
µXRF	Micro-X-ray fluorescence
NPs	Nanoparticles
PBS	Phosphate-buffered saline
PDMS	Poly(dimethylsiloxane)
PFH	Perfluorohexane
QDs	Quantum dots
RR	Ruthenium red
SC-ICP-MS	Single-cell inductively coupled plasma mass spectrometry
SIMS	Secondary ion mass spectrometry
SNMS	Secondary neutral mass spectrometry
SOD	Superoxide dismutase
SP-ICP-MS	Single particle inductively coupled plasma mass spectrometry
SR-nXRF	Synchrotron radiation nano-X-ray fluorescence
SXRF	Synchrotron X-ray fluorescence
TEM	Transmission electron microscopy
TOF-SIMS	Time-of-flight secondary ion mass spectrometry

10.1 Introduction

An integrated approach of biometal sciences called metallomics is now a well-established research field aimed at understanding the biological functions of metal ions and their chemical structures in biological systems and how their usage is fine-tuned in biological species and in populations of species with genetic variations. In fact, chemistry and biology are expected to come together in investigations of biometals because neither establishing only structures nor finding only functions is sufficient (Maret 2016).

Cells are the basic building blocks of all living organisms; they provide structure for the bodies, take in nutrients, convert them into energy, and carry out specialized functions. Thus, study of these "basic units of life" can be considered one of the most important areas of research helping understand how organisms function and how cellular components work together to carry out life functions and enable organisms to meet their basic needs.

Most known biological processes depend on metals, and, as a result, the entirety of metal ions present in a cell, including, e.g., Mg, Ca, Mn, Fe, Cu, and Zn, determines its life functions; cells use the physicochemical properties of metal ions to control essential processes. Complexation with metals is a basic functionalization reaction of cell components such as proteins (proteome), metabolites (metabolome), and nucleic acids (genome). Based on their physicochemical properties, metals are recognized, classified, and localized by living cells and then distributed to organelles – such as nuclei and mitochondria – to enable them to perform their functions.

Metallomics on the level of single cells seems to be an ultimate goal in the development of the field. Although the establishment of metallomics as a stand-alone scientific field had at its beginnings the study of individual cells (salmon eggs) by Haraguchi et al. (2008), technical limitations have been hampering more advanced investigations at this level due to small size of cells of interest in biological studies; the work with tissue homogenates (or slices in elemental imaging) has been privileged. However, it has to be underlined that cell disruption during sample preparation process (homogenization) results in loss of individual cell properties and mixing cell compartments in a way that is not likely to occur in Nature. For these reasons, development of analytical strategies for characterization of metallome homeostasis at cellular level is necessary for full understanding of life processes. Moreover, studies of individual cells in their integrity undoubtedly possess a philosophical appeal of the fundamental primary approach to explore a microcosm encapsulating the essence of life.

The first step in this direction is the determination of total element contents in individual cells. It has been suggested that correlating gene mutations, physiological status, and stress response with the trace element pattern should be carried out on the single-cell level because due to the variability of cells bulk analysis may be not meaningful (Schmid et al. 2010). The technical feasibility of such determination requires a combination of high metal detection sensitivity combined with ultrafast data acquisition. Its realization, based on the concept similar to that proposed by Tanner's group (Bandura et al. 2009) in their mass cytometry scheme of inductively coupled plasma time-of-flight mass spectrometry (ICP-TOFMS) investigation of individual cells containing metal-labeled species, has been facilitated by new instrumental developments in ICP-MS. They include systems originally designed for the analysis of nanoparticles by single-particle ICP-MS as well as miniaturized on-chip sample introductions setups. Multielemental (and multiisotopic) capability of ICP-MS allows a holistic view of cell microcosms with a perspective to study isotopic distribution and fractionation variability which is expected to bring new insights into metal utilization by the Nature.

The total element analysis is complemented by the development of intracellular metallome imaging techniques such as nanoSIMS (secondary ion mass spectrometry), synchrotron X-ray fluorescence microscopy (SXRF), and, to some extent, laser ablation (LA)-ICP-MS. NanoSIMS analysis can be performed at lateral resolution down to 50 nm thus allowing imaging at subcellular level. This methodology, based on the coaxial design of the ion gun and the secondary ion extraction, allows the analysis of up to seven ions with multicollection and recently developed oxygen probe made possible the detection of most of the metals (Nuñez et al. 2018; Pett-Ridge and Weber 2012). Another powerful tool for measuring element localization is SXRF based on a spectroscopic analysis of the emission of characteristic fluorescence from a material that has been excited by bombarding with high-energy X-rays. A new (third) generation synchrotron sources, providing high brilliance at high photon energies and highly advanced X-ray focusing systems, make it possible to visualize intracellular element localization at the sub-100 nm scale. In the case of nanoSIMS, only square-element mapping is possible (depending on the implementation energy – up to a few nanometers), while in the case of SXRF, the whole depth of the cell (up to few μm) is accessible. Another, by far more robust and easier accessible option, is laser ablation ICP-MS offering, however, worse resolution of down to several μm (Gundlach-Graham and Günther 2016).

Although the ultimate goal of all-species-of-all elements on a single-cell level seems still to be distant, the first reports on single-cell metabolomics and proteomics (Rubakhin et al. 2011) open a way to the characterization of metal-containing molecules at cellular levels. The success in this field is highly dependent on the development in small-scale high-resolution molecular mass spectrometry.

The present chapter summarizes the developments in metallomics studies on the level of individual cells highlighting novel approaches and, at the same time, discussing the current limitations and presenting perspectives of future progress.

10.2 Detection and Quantitative Distribution of Metals and Metal Nanoparticles at the Single-Cell Level

In order to fully understand a biological system such as a cell, it is necessary to determine the trace metals within the system, due to their essential roles in biological or physiological functions. In contrast with stochastic average analysis by bulk measurements, the quantitative analysis of individual cells leads to a more sensitive representation of cell-to-cell variations of content of elements (Miyashita et al. 2017). In this context, single-cell elemental analysis is considered one of the major research fields in metallomics in the next decade (Haraguchi 2017a).

However, elemental analysis of individual cells must not be restricted to the investigation of intracellular metal ions. Engineered nanoparticles are already present in our daily life in a number of consumer and industrial products from where they are directly released and incorporated into the environment. As a result, analytical methods to study their uptake by biological systems and, more specifically, by cells are needed.

In recent years, detection and quantitative multielement analysis in a single biological cell has been carried out using various measurement systems. Different applications reported in literature are shown in Table 10.1.

One of the first multielemental analyses in single biological cells was reported by Haraguchi et al. (2008). In this study, two or three salmon eggs were decomposed with HNO_3 by using a microwave-assisted acid digestion method and subsequently analyzed by ICP Atomic Emission Spectrometry (ICP-AES) and ICP-MS. In the experiment, 78 elements were the target of analysis. Sixty-six elements out of these 78 were determined in salmon egg cells, whereas other 7 elements (Li, Zr, Nb, Hf, Ir, Bi) could be only detected close to their detection limit as a result of their low abundance in the sample. The other 5 elements (F, Rh, Te, Ta, Re) were below their detection limit and they could not be determined or detected in this study. However, all these elements except F were detected in a recent experiment by using High Resolution ICP-MS (Haraguchi 2017b). The results supported the concept of the extended all present theory of the elements in a single biological cell, i.e., "cell microcosm," which postulates the existence of all elements in a single biological cell (Haraguchi 2004). Nevertheless, it has to be taken into account that the size of salmon eggs is bigger than the normal biological cells of study (mm vs µm), which requires the use of higher sensitive techniques.

More recently, Umemura et al. (2017) recently reported a multielement quantitative determination (more than 30 elements) of prokaryotic and eukaryotic cells and subcellular organelles, by microflow injection (µFI)-ICP-MS. Preliminary studies performed by ICP-MS in time-resolved mode only allowed the determination of a few major elements, such as P, Mg and Fe, whereas the signal of the other elements

Table 10.1 Summary of analytical methods for quantitative distribution and imaging analysis of single cells

Type of cell	Analytical technique	Analyte	Analytical information	Ref
Salmon eggs	ICP-AES/ ICP-MS	78 elements	Elemental content	Haraguchi et al. (2008)
Bacteria (*E. coli*) Cyanobacteria (*Synechocytis* sp.) Chlorella (*Chlorella kessleri*) Organelles	ICP-MS	>30 elements	Elemental content	Umemura et al. (2017)
Mouse fibroblasts (L929) Human pancreas (SR-4-SH) Human umbilical vein endothelial (HUVEC)	Single-cell ICP-AES	Ca	Elemental content	Nomizu et al. (1994)
Bacteria (*Bacillus subtilis*)	Single-cell ICP-SFMS	U	Uptake	Li et al. (2005)
Unicellular alga (*Chlorella vulgaris*)	Single-cell ICP-MS	Mg, Mn, cu, Cr	Elemental content	Ho and Chan (2010)
Bacteria (*Helicobacter pylori*)	Single-cell ICP-MS	Mg, bi	Uptake	Tsang et al. (2011)
Mouse leukemic monocyte macrophage (RAW 246.7)	Single-cell ICP-MS	Quantum dots	Uptake	Zheng et al. (2013)
Human cervical cancer (HeLa) Normal human bronchial epithelial (16HBE)	Single-cell ICP-MS	Gd@ $C_{82}(OH)_{22}$ CisPt	Uptake Elemental content	Zheng et al. (2015)
Human cervical cancer (HeLa) Human lung carcinoma (A549) Normal human bronchial epithelial (16HBE)	Single-cell ICP-MS	Fe, cu, Zn, Mn, P, S	Elemental content	Wang et al. (2015)
Ovarian cancer (CP70, A2780, CAOV3)	Single-cell ICP-MS	CisPt AuNPs Cu, Zn	Uptake Elemental content	Amable et al. (2017)
Yeast (*Saccharomyces cerevisiae*)	Single-cell ICP-MS	Mg, P, Ca, Mn, Fe, cu, Zn	Elemental content	Groombridge et al. (2013)
Yeast (*Saccharomyce cerevisiae*) Cyanobacterium (*Synechocystis* sp. *PCC 6803*), red algae (*Cyanidioschyzon merolae 10D* and *Galdieria sulphuraria*), green alga (*Chlamydomonas reinhardtii CC-125*)	Single-cell ICP-MS	C, mg, Al, P, S, K, Ca, Cr, Mn, Fe, Zn	Elemental content	Miyashita et al. (2014b)
Yeast (*Saccharomyce cerevisiae*)	Single-cell ICP-SFMS	Na, mg, Fe, cu, Zn, se	Elemental content	Shigeta et al. (2013a)
Unicellular alga (*Pseudococcomyxa simplex*)	Single-cell ICP-AES	Ca, mg, Fe	Elemental content	Ishihara et al. (2015)

(continued)

Table 10.1 (continued)

Type of cell	Analytical technique	Analyte	Analytical information	Ref
Bovine/calf red blood	Single-cell ICP-MS	Fe	Elemental content	Verboket et al. (2014)
Human liver carcinoma (HepG2)	Single-cell ICP-MS	ZnO NPs	Uptake	Wang et al. (2017b)
Bacteria (*Pseudomonas putida* KT2440)	CyTOF	Ru, CisPt, Ag, AgNPs	Detection and quantification	Guo et al. (2017)
Mouse fibroblasts (3 T3)	LA- ICP-SFMS	AuNPs AgNPs	Quantification Intracellular distribution	Drescher et al. (2012)
Mouse fibroblasts (3 T3) Mouse macrophages (J774)	LA- ICP-SFMS Cryo-XT	AuNPs AgNPs SiO_2NPs	Uptake Intracellular distribution	Drescher et al. (2014)
Mouse leukemic monocyte macrophage (RAW 246.7)	LA-ICP-MS	AuNPs	Uptake	Wang et al. (2013)
Marine microalgae (*Scrippsiella trochoidea*)	LA-ICP-MS	Cu	Uptake Intracellular distribution	Van Malderen et al. (2016a)
Mouse fibroblasts (3 T3)	LA-ICP-MS	AuNPs	Intracellular distribution Quantification of nanoaggregates	Büchner et al. (2014)
Paramecium	Fs-LI-O-TOFMS	Na, mg, Al, K, Ca, Mn, Fe, cu, Zn, Cs	Elemental composition	Gao et al. (2013)
Human regulatory macrophages (from CD14$^+$ monocytes)	LA-ICP-MS	AuNPs	Tracking single cells	Managh et al. (2013)
Alga (*Chlorella kesslerii*)	NanoSIMS	Cu	Intracellular distribution	Slaveykova et al. (2009)
Hyperaccumulator plant (*Alyssum lesbiacum*)	NanoSIMS	Ni, K, mg, Na, Ca	Intracellular distribution	Smart et al. (2010)
Bacterium, strain GFAJ-1	NanoSIMS	As	Intracellular distribution	Wolfe-Simon et al. (2011)
Human breast adenocarcinoma	NanoSIMS	Au	Intracellular distribution	Wedlock et al. (2011)
Human liver carcinoma (HepG2)	NanoSIMS	CuNPs	Intracellular distribution	Audinot et al. (2013)
Chlamydomonas reinhardtii and *Arabidopsis thaliana*	NanoSIMS	Na, Ca, Fe, Mn, cu	Intracellular distribution	Malherbe et al. (2016)
Marine microalgae (*Scrippsiella trochoidea*)	X-ray fluorescence	Cu, Ni, Zn, Mn	Uptake Intracellular distribution	Vergucht et al. (2015)
Fungus (*Heliscus lugdunensis*)	X-ray fluorescence	Cd	Intracellular distribution	Isaure et al. (2017)

(continued)

Table 10.1 (continued)

Type of cell	Analytical technique	Analyte	Analytical information	Ref
Microalga (*Chlamydomonas reinhardtii*)	X-ray fluorescence	Cd	Intracellular distribution	Penen et al. (2017)
Mouse fibroblasts (3 T3)	X-ray fluorescence	Zn, cu, Fe	Intracellular distribution	McRae et al. (2013)
Green microalgae (*Coccomyxa actinabiotis*)	X-ray fluorescence	Au	Intracellular distribution	Leonardo et al. (2014)
Human intestinal epithelial (HT29 – MD2)	X-ray fluorescence	Mn	Intracellular distribution	Mathieu et al. (2017)
Human fibrosarcoma (T1080)	X-ray fluorescence	Ni	Intracellular distribution	Szyrwiel et al. (2015)
Bovine ovaries	X-ray fluorescence	Se	Intracellular distribution	Ceko et al. (2015)
Pea (*Pisum sativum*) embryo	X-ray fluorescence	Fe	Intracellular distribution	Roschzttardtz et al. (2011)
Hyperaccumulator (*Arabidopsis halleri*) and non-accumulator (*Arabidopsis lyrata*) leaves	X-ray fluorescence	Cd	Intracellular distribution	Isaure et al. (2015)
Human macrophages (THP-1)	Laser-SNMS	AgNPs	Intracellular distribution	Haase et al. (2011)
Rat kidney epithelial (NRK)	TOF-SIMS	SiO_2 particles	Intracellular distribution	Hagenhoff et al. (2013)

could not be distinguished from the single produced by the background. As a result, an alternative approach was proposed, based on traditional solution-based ICP-MS after microwave-assisted acid digestion of less than 10 mg of dry weight sample. The concentration determined by ICP-MS was normalized as number of atoms per cell or organelle.

10.2.1 *Time Resolved ICP-MS Analysis*

In recent years, time-resolved ICP-MS, known as single-cell ICP-MS (SC-ICP-MS), has attracted a great deal of interest for multielemental analysis of single cells as an alternative of classical bulk analysis of large amounts of cells with a lysis, extraction, or digestion (Miyashita et al. 2014a, 2017; Mueller et al. 2014; Wang et al. 2017a). This technique is able to detect and quantify metallic elements in individual cells with high sensitivity, with the advantage of obtaining information about cell-to-cell variations instead of the average information from large cell populations obtained by conventional bulk measurements.

SC-ICP-MS is based on the well-established technique of single-particle ICP-MS (SP-ICP-MS), whose theoretical basis was outlined by Degueldre and Favarger (2003) and further developed by Laborda et al. (2014), that has shown that information about the particle size and particle number concentration can be derived from the time-resolved signals. Briefly, a cell suspension is introduced into the plasma (via conventional concentric nebulizers or other dedicated introductions systems as it will be discussed later) where droplets containing cells are vaporized and the intrinsic metals inside the cell are atomized and ionized, producing an ion plume that is detected by the ICP-MS as a short transient signal or a spike signal (also called cell event).

Each individual cell produces its own ion plume with a typical duration in the range of 100–500 μs (Miyashita et al. 2017). If the acquisition time (i.e., dwell time) of the detector is longer than the duration of the ion plume generated, signals corresponding to individual cells can be detected as high spikes, whose signal is proportional to the amount of metals in the cell. Therefore, the spike intensity distribution can be correlated with the mass distribution of the metal in the cells. On the other hand, if the dwell time is shorter than the duration of the ion plume, cells events are recorded as transient signals. In SC-ICP-MS an essential requirement is that each cell event corresponds to the signal generated by an individual cell, so that cells must be well separated in time and space in the ICP.

One of the first studies on single-cell introduction into ICP in time-resolved mode was performed by Nomizu et al. (1994). They used a previously developed airborne particle analyzer (Nomizu et al. 1992, 1994) to determine the calcium content in some single mammalian cells with diameters from 10 to 20 μm by ICP-AES. Droplets containing cells were dried in a drying chamber, and cells were directly introduced into the plasma and the calcium signal produced by each cell registered by the analyzer. For quantitative purposes, the system was calibrated with monodisperse calcium acetate aerosols generated by a vibrating orifice aerosol generator, assuming that a cell and a particle behave the same way in the plasma and thus the pulse signals derived from both produced the same pulse height if the calcium content is the same. Through this approach, they determined the calcium content in mouse fibroblasts, human pancreas, and human umbilical vein endothelial cells, with measured contents ranging from 0.057 to 0.27 pg of Ca per cell. The detection limit was reported at ~0.01 pg of Ca in a cell. However, other major elements present in cells, such as Mg, K, and Na, could not be detected due to the system that was not sensitive enough, a problem that authors thought could be overcome by using ICP-MS as detection method. In addition, the introduction efficiency of dried cells into the ICP was less than 0.1%.

The direct analysis of a single bacteria cell by SC-ICP-MS was reported for the first time by Houk's group (Li et al. 2005). *Bacillus subtilis* (*B. subtilis*), grown in a spiked uranium medium, were introduced by a microconcentric nebulizer, and the U signal incorporated intrinsically into single cells was registered by a magnetic sector instrument (ICP-SFMS) operating at the fastest integration time (4 ms). The study showed that bacteria cells behave more like large particles rather than wet droplets. U^+ spikes were observed when introducing the sample as dry and wet bacterial aerosols. On the other hand, they also showed that the U response is different for lysed and unlysed bacteria, observing a 30% increase when bacteria are lysed by sonication. The quantification of U was possible by using an inorganic U standard but applying a correction factor that has to be known.

Ho and Chan (2010) used a conventional pneumatic V-groove nebulizer to perform a single-cell analysis of a unicellular alga (*Chlorella vulgaris*, 1–6 μm) using single quadrupole ICP-MS at its lowest integration time (10 ms). This model alga was chosen as a model due to its high magnesium content. By monitoring this major element and counting the number of spikes, the number density of the cells was determined. The sample uptake rate and the algae number density were optimized to ensure that each magnesium spike corresponded to one cell. However, the transport efficiency was estimated at 0.54% due to an inefficient sample introduction system. On the other hand, they demonstrated the feasibility of a quantitative determination of Mg in the algal cells by using MgO particles for calibration. Alternatively, a semiquantitative measurement was also possible by using aqueous standards for calibration. The use of MgO particles for calibration reduces the error due to a different diffusion loss of Mg atoms coming from cells with respect to those coming from aqueous standards. Apart of the presence of a major element like Mg (10^8 atoms per cell), they were able to detect other trace elements in the algal cells, like Mn and Cu ($5x10^6$ atoms per cell). The method was also applied to a kinetic study of the sorption rate of Cr onto algal cells without separation of the cells from the original suspension.

The same group used a similar approach to obtain valuable biologically relevant info about the uptake of bismuth-based drugs in single cells (Tsang et al. 2011). The magnesium and bismuth content in *Helicobacter pylori* was monitored at the single-cell level in order to track the presence of individual cells and the metallodrug uptake. For quantitative purposes, MgO particles were used as calibration standards as in their previous work (Ho and Chan 2010). A magnesium content of about 2.9×10^7 atoms per cell was determined in wild-type bacteria, whereas the bacteria treated with the bismuth-based drug deposited nearly 1×10^6 atoms per cell. The study showed that tracking the changes of bismuth content in single bacteria cell with time provides a snapshot of bismuth uptake. Moreover, the competitive effect of ferric ions against the bismuth uptake by cells was demonstrated.

Zheng et al. (2013) applied SC-ICP-MS to determine intracellular quantum dots (QDs) in single mouse leukemic monocyte macrophage cells (RAW 246.7) after different exposure times. They used a microconcentric nebulizer to directly introduce the cells after exposure with carboxyl CdSeS of 7 nm, and the cadmium signal was monitored with a dwell time of 5 ms by using a single quadrupole ICP-MS. The method was applied to study uptake kinetics of QDs by incubating the cells for 2–12 h. A transport efficiency of 2.9% was obtained for this study. The CdS uptake was quantified by using a semiquantitative approach based on the introduction of a cadmium standard solution for calibration, assuming that ions from QDs and dissolved ions from standard solution behave alike in the plasma. A suspension of QDs of the same diameter could be not be used for calibration purposes, since 7 nm is below the size detection limit of the technique. The results were validated by flow cytometry and cell digestion methods.

The same system was used to determine the uptake of Gd@$C_{82}(OH)_{22}$, a new nanomaterials antitumor agent, and cisplatin in single cells (Zheng et al. 2015). Cancer cells (HeLa) and normal cells (16HBE) were incubated with Gd@$C_{82}(OH)_{22}$ and cisplatin at different doses for 2 and 24 h and directly introduced into the ICP after treatment, monitoring the gadolinium and platinum signals. Standard solutions of Pt or Gd were used to quantify the number of atoms per cell after each exposure dose and exposure time. Metal contents ranging from 0.03 to 2.4 pg and from 0.15 to 25 pg were obtained for Pt and Gd, respectively. Results showed that Gd@$C_{82}(OH)_{22}$ has higher bioavailability.

SC-ICP-MS was used to analyze at the single-cell level the contents and distribution patterns of essential mineral elements (Fe, Cu, Zn, Mn, P, and S) in two types of cancer cells (HeLa and A549) and one type of normal cells (16HBE) (Wang et al. 2015). Analyses were performed by using a concentric PFA-ST nebulizer which resulted in low cell transport efficiency (~0.2%). In order to fulfill the criteria that each spike signal corresponds to one cell event, dwell time and cell number density were optimized. As expected, different distribution patterns of the elements among the three types of cells were observed, which led the authors to the conclusion that these discrepancies can be used to distinguish between normal and tumor cells in mixed populations. The quantitative analysis of the elements in single cells was performed by the use of standard solutions.

Amable et al. (2017) used SC-ICP-MS to investigate the uptake of cisplatin by ovarian cancer cells, by tracking the platinum content in individual cells over time, which could be used as a predictor of the effectiveness of the treatment. The platinum content increased over time, signifying increased cisplatin uptake. Moreover, the same authors used the same analytical approach to study the uptake rate of gold nanoparticles (AuNPs) at two different concentrations by three different ovarian cell lines and to determine the intrinsic copper and zinc contents in one ovarian cell line. In the later study, the use of a short dwell time (50 μs) allowed to reduce the background signal while keeping the signal-to-background ratio constant.

One of the major drawbacks of SC-ICP-MS is the high sample consumption (as a consequence of inefficient cell transport efficiency) in conventional sample introduction systems, usually based on a concentric nebulizer and a spray chamber. As we have seen in the previous studies reported, the cell transport efficiency was <5%. In order to try to overcome this problem, some groups have developed special sample introduction devices.

Groombridge et al. (2013) developed a high-efficiency cell introduction system (HECIS), which was based on a total consumption sample introduction device, to determine trace elements in single yeast cells (*Saccharomyces cerevisiae*). The sample introduction system consisted of a modified high performance concentric nebulizer (HPCN) and a 15 mL on-axis spray chamber utilizing a sheath gas glow to prevent sample deposition. Besides, a solution of NaCl at low concentration was added to the cell suspension in order to reduce cell adsorption. The modified nebulizer was able to generate aerosols below 10 μm in size by working at 10 μL min^{-1}, which leads to a lower background noise level. With the developed system, a cell transport efficiency of 75.0 ± 4.7% into the plasma was achieved for the analysis of single yeast cells. The signals of Mg, P, Ca, Mn, Fe, Cu, and Zn were obtained by single quadrupole ICP-MS at a dwell time of 10 ms. They also conducted a preliminary investigation into the potential for multielement correlation analysis within cells by using ICP-TOFMS. The time-resolved profiles of six elements (Mg, P, Mn, Fe, Cu, and Zn) were simultaneously obtained in one measurement at a dwell time of 1 ms. Results show a relatively strong correlation for the spectra between P and Zn (correlation factor, 0.69), between P and Mg (0.63), and between Mg and Zn (0.63). Despite the successful application of the HECIS, the cell transport efficiency was not close to 100%, probably due to cell loss during introduction, according to the author (Miyashita et al. 2014b). Therefore, the same group modified the HPCN in order to improve the efficiency of single-cell analysis by reducing the loss of cells, as well as to accept a wider range of size cells (from 2.0 to 6.4 μm) (Miyashita et al. 2014b). The modified system consisted of an HPCN with a large-bore center capillary tube (LB-HPCN) and a 15 mL on-axis spray chamber still with a sheath gas flow but with a longer total length and shorter inner tube length. Besides, an external ion pulse counting unit allowed improving the data acquisition frequency (0.05–1 ms). The system was tested by monitoring a wide range of biologically important elements (C, Mg, Al, P, S, K, Ca, Cr, Mn, Fe, Zn) in unicellular microbes of different sizes: yeast (*Saccharomyces cerevisiae*), cyanobacterium (*Synechocystis* sp. *PCC 6803*), red algae (*Cyanidioschyzon merolae 10D* and *Galdieria sulphuraria*), and green alga (*Chlamydomonas reinhardtii CC-125*). The cell introduction efficiencies determined ranged 86% to ca. 100% for microbes with cell diameter of 6.4 mm and 2.0–3.0 mm, respectively.

A sample introduction system based on micro-droplet generator (μDG) was developed by Shigeta et al. (2013a) and coupled to a sector field ICP-MS instrument, operating in fast scanning mode (shortest dwell time of 100 μs). Uniformly sized droplets down to 23 nm were achieved thanks to the use of triple pulse mode of the droplet generator. The generated droplets were injected into a low-temperature desolvation system, using He as drying gas. The system was successfully applied for the detection of trace elements (Na, Mg, Fe, Cu, Zn, Se) in single selenized yeast cells (*Saccharomyce cerevisiae*) with 100% transport efficiency (Shigeta et al. 2013b). The single yeast cells with a diameter of roughly 6 μm were embedded into droplets and introduced into the plasma, with a fixed droplet generation rate of 50 Hz, producing equidistant signals that allowed the discrimination between signals produced due to background form those produced by the analyte. Signal intensities from single cells were measured for Cu, Zn, and Se from the histograms for about 1000 cell events. In addition, they performed open vessel digestion of washed yeast cells for multielement analysis, determining absolute amounts per single cell for Na (0.91 fg), Mg (9.4 fg), Fe (5.9 fg), Cu (0.54 fg), Zn (1.2 fg), and Se (72 fg).

Ishihara et al. (2015) developed a desolvation system for micro-droplet injection system (M-DIS) in order to detect trace metals in the unicellular alga *Pseudococcomyxa simplex* by ICP-AES. In the M-DIS system, the cell solution is not nebulized but introduced at the center of the ICP as a single micro-droplet with a diameter between 30 and 70 μm. The desolvation system readily removed the water vapor by placing a cooling part to the introduction route downstream of the heating, allowing the decrease of the solvent load in the droplet and thus improving the sensitivity of the elements present in the cell. The modified M-DIS system equipped with the desolvation system was coupled to ICP-AES, and the emission spectra of Ca, Mg, and Fe contained in a single cell were recorded; however, the emission spectra corresponding to the metals Mn, Zn, and Mo could not be detected.

Verboket et al. (2014) proposed a novel droplet microfluidic sample introduction system for ICP-MS. The system is based on a liquid-assisted droplet ejection (LADE) chip made entirely of poly(dimethylsiloxane) (PDMS), which produced droplets in a stream of perfluorohexane (PFH). A membrane desolvator is used prior the injection into the plasma to reduce the droplet size. The chip was able to generate highly monodisperse droplets in the size range from 40 to 60 μm, which remain intact during the ejection and can be transported and directly injected into the ICP with >50% efficiency. The system was tested by introducing calf red blood cells suspended in phosphate-buffered saline (PBS) and monitoring the ^{56}Fe signal. However, the transport efficiency of cells was low (4.5%) as a result of losses in the transport assembly. The amount of Fe per cell was calculated by calibrating the instrument with droplets consisting of a multielement solution.

Recently, Wang et al. (2017b) fabricated a droplet chip which produced droplets with an average diameter of 25 μm, online with an ICP-MS via a microflow nebulizer. The single cells encapsulated in the droplets generated by the chip remained intact during its transportation from the outlet of the droplet chip to the microflow nebulizer. The developed droplet chip was applied for the quantification of Zn and zinc oxide nanoparticles (ZnO NPs) uptake/adsorption in single HepG2 cells by SC-ICP-MS. ZnO NPs were used for the quantification of Zn in single cells. The cell transport efficiency was low (2.96%) compared with other systems, but the frequency of droplet generation was high ($3–6 \times 10^6$ droplets per minute).

Mass cytometry, usually in combination with a time-of-flight analyzer, can offer the capability of single-cell analysis on the basis of specific metal-based cell markers. Tanner's group introduced in 2008 for the first time a specialized system for the multiparametric analysis of single cell at high throughput (Bandura et al. 2009, Tanner et al. 2008). The developed system was used for the analysis of human cells through an approach based on multiatom elemental antibody tagging. The mass cytometer was later introduced to the market as "CyTOF" by DVS Sciences Inc.

More recently, Guo et al. (2017) used CyTOF for label-free detection and quantification of Ag in single bacterial (*Pseudomonas putida*) cells of different physiological states. Cells were treated with silver ions or 10 nm silver nanoparticles (AgNPs). The amount of Ag per cell was determined via the intensity of the mass cytometric signal for Ag. The information about the amount of Ag per cell was combined with an approach using ruthenium red (RR) staining as a marker for all cells of a population and cisplatin staining for live/dead cell discrimination. They found that the treatment with AgNPs caused higher frequencies of dead cells, higher frequencies of Ag-containing cells, and higher per-cell silver quantities.

10.2.2 Other MS-Based Approaches

Apart of its capabilities to obtain information about the intracellular distribution of metal and metal nanoparticles, as it will be discussed in the next section, LA-ICP-MS is able to provide quantitative information. In this context, LA-ICP-MS allows the quantification of inorganic nanoparticles without losing spatial information of the nanoparticle distribution at the cell level, overcoming the disadvantages of ICP-MS elemental analysis after cell digestion or extraction.

One of the major problems to achieve an accurate quantification of metals and metal nanoparticles by LA-ICP-MS is a lack of suitable single-cell standards. In order to overcome this problem, different approaches have been investigated.

Drescher et al. (2012) used LA coupled to a sector field ICP-MS to study the uptake of AuNPs (with a diameter of 25 nm) and AgNPs (with a diameter of 50 nm) in single eukaryotic cells (mouse fibroblasts). The number of nanoparticle per cell after incubation was determined on the basis of a matrix-matched calibration using nitrocellulose membranes spiked with nanoparticle suspension. The limit of detection and the limit of quantification for AgNPs were 20 and 60 particles and for AuNPs were 190 and 550 particles, respectively. Results showed a strong dependency of particle uptake on concentration and incubation conditions. In the case of AgNPs, increasing nanoparticle concentration and incubation time was shown to lead to an increase of the silver intensity inside the cells, which was directly correlated with an increasing number of nanoparticles.

The same group used LA-ICP-MS for a quantitative comparison of the uptake of uncoated AgNPs and AuNPs, silica-coated AgNPs, and silica nanoparticles with a plasmonic (Au or Ag) core (BrightSilica) by single mouse fibroblasts and macrophages (Drescher et al. 2014). The use of nanoparticles with thicker shells (silica-coated AgNPs) provided the possibility to compare the uptake of relatively large nanoparticles with smaller ones (BrightSilica with thin shells) at an identical size of the plasmonic cores. Since the uptake of nanoparticles by cells is size dependent, the signal intensity obtained was about six times higher for BrightSilica(Ag) with a diameter of 57 nm than for the 126 nm silica-coated AgNPs. Results also showed a smaller uptake by fibroblast cells of BrightSilica NPs in comparison with uncoated AgNPs and AuNPs of almost the same size.

Wang et al. (2013) quantified the gold mass in single mouse leukemic monocyte macrophage cells (RAW 246.7) exposed to 30 nm AuNPs by LA-ICP-MS. For calibration purposes an inkjet printer producing dried residues of picoliter droplets was used in order to simulate matrix-matched calibration standards. Under controlled conditions, the droplets dispensed from the printer were almost identical with less than 1% mass variations. Through this calibration approach, a limit of quantification of 1.7 fg Au was achieved. A log-normal distribution, ranging from 1.7 to 72 fg Au per cell, corresponding to 9 to 370 AuNPs per cell, was obtained in single cells exposed to AuNPs for 4 h.

Van Malderen et al. (2016a) presented an interesting quantitative approach in order to overcome the limitations in precision, accuracy, and efficiency of current calibration strategies in LA-ICP-MS. For this purpose, they designed and proposed the use of high-density microarray plates for multiple matrix-matched standards. A calibration curve with good linear correlation was obtained within the range of 5–200 µg g^{-1}, exhibiting a detection limit of 3 fg Cu. The system was applied for the quantification at the single-cell level of Cu in the marine microalgae *Scrippsiella trochoidea* after copper exposure.

Büchner et al. (2014) studied the accumulation of AuNPs in fibroblast cells during cellular uptake, processing, and mitosis. Cells were exposed to 14 nm AuNPs with different incubation times and analyzed by LA-ICP-MS. Results showed that AuNPs form aggregates of different sizes, and the gold signal intensity can be compared for the different incubation times. As an indicator for the aggregation of nanoparticles inside the cells, the authors determined the number of spots per cell with a gold signal intensity >50,000 cps. The number of spots with gold intensity >50,000 cps showed a different trend that was attributed to a change in the intracellular particle distribution over time.

Finally, Gao et al. (2013) proposed an approach based on high irradiance femtosecond laser ionization orthogonal time-of-flight mass spectrometry (fs-LI-O-TOFMS) to determine the elemental composition of single paramecium cells, with the size of several tens of micrometers. After a simple preparation procedure, based on heating and drying the cells, a series of elements (Na, Mg, Al, P, S, Cl, K, Ca, Mn, Fe, Cu, Zn, I, Cs) were determined in paramecium at the pg per cell level. Salts of these elements were used in order to increase the element concentration. This approach allowed the measurement of nonmetallic elements like P, S, or Cl difficult to analyze with single quadrupole ICP-MS instruments. An absolute limit of detection (ALOD) at the femtogram level was achieved.

10.3 Subcellular Distribution Analysis of Metal and Metal Nanoparticles in Single Cells by Imaging Techniques

As it has already been mentioned, classical studies of biological cells consist on the digestion of a cell suspension and thus averaging over a huge number of cells. With this approach, not only the intrinsic individual variation but also the information about intracellular distribution of metals is lost. Nevertheless, each cell is subdivided into different compartments with specific reactions, and thus chemical elemental imaging is critical to elucidate the biochemical processes that take place in each of them.

The determination of the metal distribution at the subcellular level in individual cells is challenging and requires analytical methods with high sensitivity and high spatial resolution. In the last years, the advances in analytical techniques like LA-ICP-MS, SIMS, or SXRF have opened a number of possibilities for imaging at the single-cell level. Different applications reported in literature are shown in Table 10.1.

10.3.1 LA-ICP-MS

LA-ICP-MS is an established quantitative elemental analysis and mapping technique, which provides spatially resolved information on element distribution (qualitative and quantitative) in biological samples (Mueller et al. 2014). Rapid response LA-ICP-MS systems greatly benefit throughput and sensitivity, which are key parameters in 2D and 3D imaging at high lateral resolution (Van Malderen et al. 2016b). The novel capabilities of laser ablation as a sample introduction technique in ICP-MS are being increasingly applied for advanced imaging mass spectrometry.

LA-ICP-MS was used by Managh et al. (2013) for tracking single macrophage cells labeled with 50 nm AuNPs in different tissues of immunodeficient mice. Since the cell diameter (~10 μm) was much smaller than the laser spot diameter (25 μm), a single cell was completely ablated in each laser shot.

Jakubowski's group (Drescher et al. 2012, 2014) showed the capabilities of LA-ICP-MS for spatially resolved bioimaging of the intracellular distribution of nanoparticles in single eukaryotic cells in two different studies. Scan speed, ablation frequency, and laser energy were optimized in order to achieve a laser spot size of 4 μm or 8 μm so that the laser spots are widely overlapping each other and the signal of the sample is generated by the difference in the ablated area. By using this laser ablation scan mode, the lateral resolution in scan direction is much smaller than the laser spot diameter, obtaining a high-resolution image. In a first study, they used the optimized ablation system to investigate the intracellular distribution of AuNPs and AgNPs in cellular substructures of single mouse fibroblasts (Drescher et al. 2012). The subcellular mapping obtained enabled the differentiation of nanoparticles in the cytosol from those in the cell nucleus region.

In a different study, the same group combined LA-ICP-MS with cryo nanoscale X-ray tomography (cryo-XT) to investigate the intracellular distribution at the subcellular level with 3D resolution of silica nanoparticles with a plasmonic (Au or Ag) core (BrightSilica) in 3 T3 fibroblast cells and J774 macrophage individual cells (Drescher et al. 2014). Taking advantage of the absorption of soft X-rays by the silica material, the study confirmed that BrightSilica nanoparticles enter cells by an endocytotic mechanism.

Büchner et al. (2014) detected Au nanoaggregates at subcellular level in single fibroblast cells by LA-ICP-MS micromapping. They achieved high sensitivity at high spatial resolution and complete cell ablation by optimizing the laser ablation parameters as previously described in the study performed by Drescher et al. (2012). By using an 8 μm diameter beam, they showed that the nanoaggregates accumulated in localized, perinuclear regions of the cells, but it was also demonstrated that reorganization occurred during mitosis.

However, these LA-ICP-MS micromapping studies were performed in fibroblast cells, which can be considered relatively large in size (≥50 μm in diameter). Therefore, the application would benefit from improved spatial resolution for the investigation of the distribution of nanoparticles within smaller cells (Van Malderen et al. 2016a).

Van Malderen et al. (2016a) demonstrated the capabilities of LA-ICP-MS to study the intracellular transition metal distribution in single cells of model marine microalgae. Microimaging of *Scrippsiella trochoidea* exposed to 20 μg g^{-1} indicated an important organelle acting as preferential storage of Cu. These conclusions were corroborated by images obtained by SXRF in a cross-validation approach (Vergucht et al. 2015), showing the potential of LA-ICP-MS for subcellular level imaging.

While the use of LA-ICP-MS for single-cell imaging is just at its beginning, other SXRF microscopy and secondary ion mass spectrometry showed already that the imaging of biological trace metals at nm scale is possible (Qin et al. 2011).

10.3.2 NanoSIMS

SIMS is an analytical technique based on the use an accelerated primary ion beam that bombards a solid surface and generates secondary ions, which are subsequently analyzed by a mass spectrometer (Boxer et al. 2009). In the case of nanoSIMS, the primary ion beam is scanned over the surface of the sample, and ejected secondary ions are analyzed by a double sector mass spectrometer (Schaumlöffel et al. 2016).

Current nanoSIMS instruments are equipped with two different primary ions sources: a thermal ionization cesium positive ion source that generates negative secondary ions (Storms et al. 1977) and a duoplasmatron oxygen negative ion source that generates positive secondary ions (Benninghoven et al. 1987). Its high spatial resolution (better than 100 nm) has opened numerous research application fields, such as the detection of chemical elements at the subcellular level in biological samples.

Slaveykova et al. (2009) demonstrated the capabilities of nanoSIMS to investigate Cu distribution in single micrometer-sized algal cells. The microalga *Chlorella kesslerii* was exposed to nanomolar and micromolar copper concentrations, representative of natural and heavily contaminated waters, and the subcellular distribution of copper in individual cells was mapped by measuring $^{63}Cu^{-}$ and $^{65}Cu^{-}$ secondary ions. A cesium source was used to generate Cs^{+} primary ions that were accelerated as a tightly focused ion beam with a probe working diameter of approximately 50 nm. Results showed that the quantity of Cu in the cell wall and membrane was lower than that in the cell interior.

Smart et al. (2010) used nanoSIMS with dedicated sample preparation methodologies to study the distribution of nickel and other elements in single cells from a nickel hyperaccumulator plant (*Alyssum lesbiacum*), with spatial resolutions of better than 100 nm. A $^{58}Ni^{-}$ signal distribution was obtained by using the primary Cs^{+} ion beam, whereas the primary O^{-} ion beam allowed them to obtain maps showing the distribution of the positive secondary ions $^{23}Na^{+}$, $^{40}Ca^{+}$, $^{39}K^{+}$, $^{24}Mg^{+}$, and $^{58}Ni^{+}$ from the same area analyzed with the Cs^{+} beam. They demonstrated a significant sequestration of nickel in the epidermal cell vacuoles together with a uniform distribution throughout the cell walls. However, despite the sample preparation methodology applied in this study helped to minimize the redistribution of soluble elements, the in vivo distributions of highly diffusible ions ($^{23}Na^+$, $^{24}Mg^+$, $^{39}K^+$, and $^{40}Ca^+$) were significantly altered during chemical fixation.

Wolfe-Simon et al. (2011) used nanoSIMS to study the intracellular arsenic in a bacterium (strain GFAJ-1 of the *Halomonadaceae*) that is able to substitute arsenic for phosphorus to sustain its growth. Bacteria was grown in an arsenic-enriched medium, using radiolabeled $^{73}AsO_4{}^{3-}$ to obtain more specific information about the intracellular distribution of arsenic in single GFAJ-1 cells.

Wedlock et al. (2011) investigated the subcellular distribution of gold in situ in human breast cancer cells treated with an antitumor Au(I) complex. A Cs^+ primary ion beam was used for imaging the negative secondary ion $^{197}Au^-$. Different beam currents were applied to obtain primary beam diameters of ~110 nm (low-resolution images) or ~50 nm (high-resolution images). NanoSIMS maps for $^{197}Au^-$ signal in single cells after treatment showed that the subcellular distribution of gold was associated with sulfur-rich regions in the cytoplasmic, nuclear, and perinuclear regions.

The intracellular distribution of copper oxide nanoparticles (CuO NPs) in HepG2 cells was studied by Audinot et al. (2013) by nanoSIMS imaging. $^{63}Cu^-$ maps were acquired with a Cs^+ ion primary beam, and a probe diameter in the range 80–100 nm in single cells was exposed to CuO NPs (25 mg mL^{-1}) for 24 h.

The detection of many trace elements at the single-cell level by nanoSIMS requires the generation of secondary positive ions with high yield by an oxygen primary ion source. However, the commonly used duoplasmatron oxygen source cannot achieve the same lateral resolution as the cesium primary source due to a larger primary ion beam size (down to 50 nm for the Cs source and 200 nm for the duoplasmatron oxygen source) (Schaumlöffel et al. 2016). In order to overcome this problem, Malherbe et al. (2016) designed a new rf plasma oxygen source that was fitted and characterized on a nanoSIMS instrument. This new oxygen ion source was applied for the localization of trace metals (Na, Ca, Fe, Mn, Cu) in individual cells of two model organisms: a unicellular alga (*C. Reinhardtii*) and flowering plant (*Arabidopsis thaliana*). The new rf plasma oxygen primary ion source showed higher achievable lateral resolutions and higher apparent sensitivities for electropositive elements compared to the commonly used duoplasmatron source. The images produced for positive secondary ions with the rf plasma source showed similar lateral resolution to those obtained for negative secondary ions with the cesium source.

10.3.3 Synchrotron-Based X-ray Fluorescence

SXRF (also abbreviated as μXRF) is among the most powerful techniques for the investigation of metal accumulation at the cell level and can be used for imaging element distribution at high spatial resolution (<100 nm) (Roudeau et al. 2014).

This technique is based in the X-ray fluorescence energy emitted by an atom that has been previously irradiated by X-ray photons produced by synchrotron radiation (Schaumlöffel et al. 2016). The irradiated atom ejects a core electron with a characteristic binding energy. In SXRF, the sample is moved by a nano-positioner stage, and spectra are recorded pixel by pixel which enable to provide images of the distribution of metals in single cells. SRXF has been widely applied in different investigation of the metal distribution at the single-cell level. Some interesting applications of SXRF will be explained below.

Vergucht et al. (2015) reported a new imaging approach based on the combination of optical tweezer technology with synchrotron radiation confocal XRF. The method allowed elemental imaging in a 2D projection mode in single marine microalgae (*Scrippsiella trochoidea*) cells in their natural, in vivo state. The elemental distributions showed that significant amounts of Mn, Fe, Cu, and Zn were detected within the Zn-exposed algae. In addition, the in vivo areal concentrations of accumulated metals in single cells could determine in a semiquantitative way, showing larger differences (Cu > > Ni > Zn).

Elemental imaging by synchrotron µXRF was used by Isaure et al. (2017) to investigate Cd in fungal hyphae at the subcellular level. Aquatic fungus *H. lugdunensis* was exposed to 50 µM Cd and µXRF maps obtained after 5 and 7 days. Results showed that the hyphal tip cells were depleted in Cd and that the metal was stored in older cells. S and P localization was also determined.

Penen et al. (2017) studied the Cd distribution in single microalga (*Chlamydomonas reinhardtii*) cells. Three different *C. reinhardtii* strains were exposed to 70 µM Cd and analyzed by µXRF. µXRF maps from the three strains demonstrated that Cd level was highly heterogeneous between cells.

In an interesting approach, the redistribution of transition metals in mouse fibroblast cells during the individual stages of mitosis was investigated (McRae et al. 2013). Results showed similar mechanisms for the inheritance of Zn and Cu, but not Fe. Moreover, SXRF maps provided first clues toward a mechanism that might involve compartmentalized transport and possibly a role of the Golgi apparatus.

Leonardo et al. (2014) studied the subcellular location of silver and cobalt in a newly discovered unicellular microalga (*Coccomyxa actinabiotis*) by synchrotron radiation nano-X-ray fluorescence (SR-nXRF). The microalga was exposed to different concentrations of silver and cobalt, and the subcellular distribution after exposure was investigated. They found that cobalt was homogeneously distributed outside of the chloroplast, whereas silver was localized in the cytosol at low concentration and in the whole cell excluding the nucleus at high concentration.

Mathieu et al. (2017) studied the intracellular distribution of manganese in single human intestinal epithelial cells. Cells were incubated with $MnCl_2$ or the manganese complex Mn1 mimicking superoxide dismutase (SOD), a protein involved in cell protection against oxidative stress, and manganese was mapped on cryofixed freeze-dried cells using SXRF with a resolution of 200 nm. The intracellular manganese content in a single cell was higher after incubation with the manganese complex than that in the control cell, but $MnCl_2$ was more efficiently taken up. Moreover, SXRF maps demonstrated a diffuse distribution of manganese with higher amounts where the cell is the thickest.

Szyrwiel et al. (2015) used SXRF to map the intracellular nickel in human fibrosarcoma cells. Cells were incubated with Ni^{2+} or a newly Ni^{2+}-branch peptide complex (NiA), designed to deliver Ni^{2+} to the cell nucleus. SXRF images demonstrated the nuclear location of Ni in cells treated with the NiA complex. However, in cells treated with nickel ions, effective metal uptake was not observed.

Ceko et al. (2015) determined the intracellular selenium distribution in single bovine ovaries by SXRF imaging. The approach allowed localizing Se to the granulosa cell layer of large (>10 mm) healthy follicles.

Moreover, the use of SXRF has also been reported for the investigation of metal localization in plant cells (Zhao et al. 2014).

Roschzttardtz et al. (2011) studied the intracellular location of iron in single pea (*Pisum sativum*) cells by µXRF. The results revealed that, unexpectedly, the iron concentration found in the nucleus was higher than in the expected iron-rich organelles such as plastids or vacuoles. Furthermore, they showed that within the nucleus, the iron concentration in the nucleolus is the highest encountered among the intracellular compartments. This study raised the important question of the role that nucleolar iron plays in plant cells.

Isaure et al. (2015) used µXRF to investigate the distribution of cadmium in leave cells of two plants: the hyperaccumulator *Arabidopsis halleri* and the non-accumulator *Arabidopsis lyrata*. Images were obtained after 3 weeks of cadmium exposure. In the leaves of *A. halleri*, cadmium was found inside the cell and at the rim of the cell. However, the cellular distribution in *A. lyrata* leaves could not be obtained, since the lateral resolution and the cadmium were too low.

10.3.4 Other MS Approaches

The intracellular distribution of nanoparticles has also been studied through other analytical approaches based on mass spectrometry techniques.

For instance, Haase et al. (2011) tested the capabilities of laser postionization secondary neutral mass spectrometry (laser-SNMS) for the study of the intracellular distribution of peptide-coated 20 nm AgNPs inside individual human macrophages cells, comparing the results with the established confocal Raman microscopy and transmission electron microscopy (TEM). Although confocal Raman microscopy is fastest and requires a much simpler sample preparation, laser-SNMS provides a much greater sensitivity and 3D resolution limits, being capable of detecting metal atoms with a spatial resolution of down to 100 nm. The images obtained demonstrated significant accumulation of silver particles under the form of aggregates inside the cells. Laser-SNMS was used in combination with TOF-MS to follow subtle biochemical alterations related to nanoparticle treatment.

Finally, TOF-SIMS 3D analysis proved to be able to localize silica micro- and nanoparticles with sizes down to 150 nm in single rat kidney epithelial cells (Hagenhoff et al. 2013). The approach followed by Hagenhoff et al. (2013) allowed the discrimination between extracellular and intracellular localization of nonluminescent, unlabeled nanoparticles, otherwise hard to localize by other analytical techniques. TOF-SIMS provided images of their prominent distribution around the cell nucleus.

10.4 Molecular Analysis and Perspectives

The development of new analytical methods has opened the door to the identification of metabolites in single cells. One of the most interesting approaches is the coupling of high-resolution separation by capillary electrophoresis (CE) with high sensitivity and selectivity detection by electrospray ionization mass spectrometry (ESI-MS) (Týčová et al. 2017). For instance, Comi et al. (2017) developed an approach based on CE-ESI-MS to identify several amino acids as well as dopamine in single pancreatic islet cells.

On the other hand, no metalloproteomic and metallometabolomic data exist for single cells. However, in order to fully understand the cellular specificity and complexity of cells, it is necessary to measure molecular signatures with single-cell resolution (Wang and Bodovitz 2010). The future development of single-cell metallomics clearly depends on the developments in small-scale molecular mass spectrometry accompanied by custom-designed sample preparation methods. High-resolution mass spectrometry imaging, necessary for this purpose, requires a smaller region of sample for each pixel, but this sampling reduction is translated into a decrease of ionization efficiency and sensitivity (Dong et al. 2016).

SIMS is an ideal technique for mass spectrometry imaging thanks to its high surface sensitivity and submicron resolution (Passarelli and Ewing 2013). However, recent technical advances in the field of matrix-assisted laser desorption ionization (MALDI) have pushed its spatial resolution from the 20–100 μm range to the 1–10 μm range (Passarelli and Ewing 2013), reaching the point where single-cell mass spectrometry can be accomplished, although continued technology development is needed (Murray et al. 2016). For instance, Zavalin et al. (2012) developed a transmission geometry ion source which enabled to perform high-throughput MALDI MS imaging, achieving higher sensitivity. They demonstrated the capabilities of the developed method by mapping the distribution of lipids and peptides in mammalian cells with 1 μm spatial resolution opening a way to single-cell mass spectrometry imaging such as single-cell proteomic (and, in future, metalloproteomic) imaging, even though the sensitivity is still a challenge.

The analysis of large metabolites in single cells remains a challenging task. TOF-SIMS is able to provide submicrometer spatial resolution for imaging of metabolites in single cells, whereas MALDI offers a high mass resolution. However, single-cell analysis by mass spectrometry imaging is limited in mass resolution range to $m/z < 500$ in the case of TOF-SIMS and in spatial resolution (pixel size in the range of 50–200 μm) in the case of MALDI. Therefore, the analysis of metabolites and – in perspective – metallometabolites in individual cells with high spatial resolution and high mass accuracy simultaneously remains a challenge.

However, in an interesting approach, Schober et al. (2012) have already developed a high-resolution mass spectrometry single-cell imaging method. They demonstrated for the first time the combination of high spatial resolution (7 μm) with high mass accuracy (<3 ppm) and high mass resolution (R = 100,000 at m/z = 200) in imaging analysis of human cervical cancer (HeLa) cells. Analyses were performed with a high-resolution atmospheric pressure MALDI (AP-MALDI) coupled to an Orbitrap mass spectrometer. The developed method allowed them to identify larger metabolites in intact single cells thus giving a direction to future investigations of metal-binding species.

Finally, and in other to sum up, the different analytical techniques discussed in this chapter, together with the relevant information obtained, are summarized in Fig. 10.1.

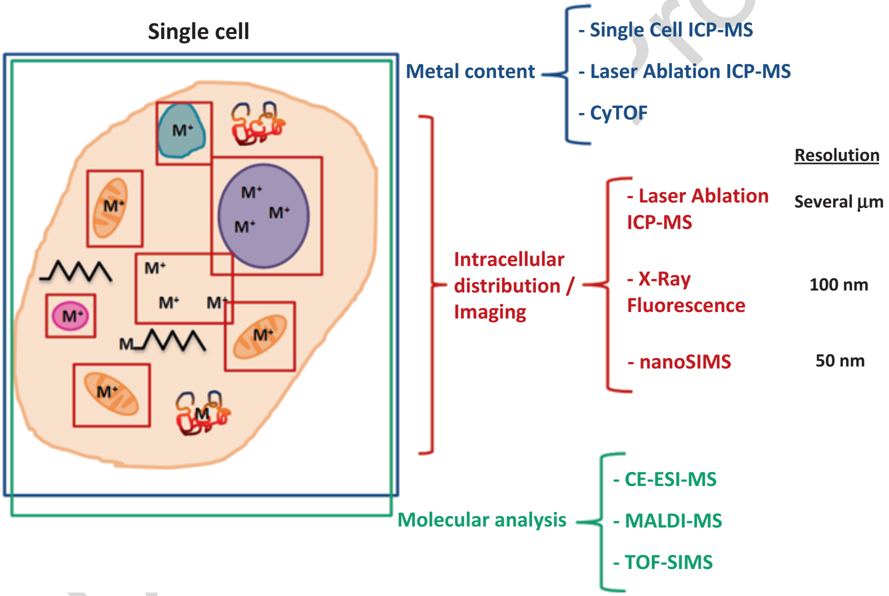

Fig. 10.1 Schematic representation of analytical information obtained by different analytical techniques at the single-cell level

References

Amable L, Stephan C, Smith S, Merrifield R (2017) An introduction to single cell ICP-MS analysis. Perkin Elmer, USA, pp 3–39

Audinot JN, Georgantzopoulou A, Piret JP, Gutleb AC, Dowsett D, Migeon HN, Hoffmann L (2013) Identification and localization of nanoparticles in tissues by mass spectrometry. Surf Interface Anal 45:230–233

Bandura DR, Baranov VI, Ornatsky OI, Antonov A, Kinach R, Lou X, Pavlov S, Vorobiev S, Dick JE, Tanner SD (2009) Mass cytometry: a novel technique for real-time single cell multi-target immunoassay based on inductively coupled plasma time of flight mass spectrometry. Anal Chem 81:6813–6822

Benninghoven A, Rudenauer FG, Werner HW (1987) Secondary ion mass spectrometry: basic concepts, instrumental aspects, applications and trends. Wiley-Interscience, New York

Boxer SG, Kraft ML, Weber PK (2009) Advances in imaging secondary ion mass spectrometry for biological samples. Annu Rev Biophys 38:53–74

Büchner T, Drescher D, Traub H, Schrade P, Bachmann S, Jakubowski N, Kneipp J (2014) Relating surface-enhanced Raman scattering signals of cells to gold nanoparticle aggregation as determined by LA-ICP-MS micromapping. Anal Bioanal Chem 406:7003–7014

Ceko MJ, Hummitzsch K, Hatzirodos N, Bonner WM, Aitken JB, Russell DL, Lane M, Rodgers RJ, Harris HH (2015) X-Ray fluorescence imaging and other analyses identify selenium and GPX1 as important in female reproductive function. Metallomics 7:71–82

Comi TJ, Makurath MA, Philip MC, Rubakhin SS, Sweedler JV (2017) MALDI MS guided liquid microjunction extraction for capillary electrophoresis – electrospray ionization MS analysis of single pancreatic islet cells. Anal Chem 89:7765–7772

Degueldre C, Favarger PY (2003) Colloid analysis by single particle inductively coupled plasma-mass spectroscopy: a feasibility study. Colloids Surfaces A Physicochem Eng Asp 217:137–142

Dong Y, Li B, Aharoni A (2016) More than pictures: when MS imaging meets histology. Trends Plant Sci 21:686–698

Drescher D, Giesen C, Traub H, Panne U, Kneipp J, Jakubowski N (2012) Quantitative imaging of gold and silver nanoparticles in single eukaryotic cells by laser ablation ICP-MS. Anal Chem 84:9684–9688

Drescher D, Zeise I, Traub H, Guttmann P, Seifert S, Büchner T, Jakubowski N, Schneider G, Kneipp J (2014) In situ characterization of SiO2 nanoparticle biointeractions using BrightSilica. Adv Funct Mater 24:3765–3775

Gao Y, Lin Y, Zhang B, Zou D, He M, Dong B, Hang W, Huang B (2013) Single-cell elemental analysis via high irradiance femtosecond laser ionization time-of-flight mass spectrometry. Anal Chem 85:4268–4272

Groombridge AS, Miyashita S, Fujii S, Nagasawa K, Okahashi T, Ohata M, Umemura T, Takatsu A, Inagaki K, Chiba K (2013) High sensitive elemental analysis of single yeast cells (Saccharomyces cerevisiae) by time-resolved inductively-coupled plasma mass spectrometry using a high efficiency cell introduction system. Anal Sci 29:597–603

Gundlach-Graham A, Günther D (2016) Toward faster and higher resolution LA-ICPMS imaging: on the co-evolution of la cell design and ICPMS instrumentation Young Investigators in Analytical and Bioanalytical Science. Anal Bioanal Chem 408:2687–2695

Guo Y, Baumgart S, Stärk H-J, Harms H, Müller S (2017) Mass cytometry for detection of silver at the bacterial single cell level. Front Microbiol 8:1–9

Haase A, Arlinghaus HF, Tentschert J, Jungnickel H, Graf P, Mantion A, Draude F, Galla S, Plendl J, Goetz ME, Masic A, Meier W, Thünemann AF, Taubert A, Luch A (2011) Application of laser postionization secondary neutral mass spectrometry/time-of-flight secondary ion mass spectrometry in nanotoxicology: visualization of nanosilver in human macrophages and cellular responses. ACS Nano 5:3059–3068

Hagenhoff B, Breitenstein D, Tallarek E, Möllers R, Niehuis E, Sperber M, Goricnik B, Wegener J (2013) Detection of micro- and nano-particles in animal cells by ToF-SIMS 3D analysis. Surf Interface Anal 45:315–319

Haraguchi H (2004) Metallomics as integrated biometal science. J Anal At Spectrom 19:5–14

Haraguchi H (2017a) Metallomics: the history over the last decade and a future outlook. Metallomics 9:1001–1013

Haraguchi H (2017b) Metallomics: integrated biometal science. In: Ogra Y, Hirata T (eds) Metallomics: recent analytical techniques and applications. Springer, Berlin, pp 3–39

Haraguchi H, Ishii A, Hasegawa T, Matsuura H, Umemura T (2008) Metallomics study on all-elements analysis of salmon egg cells and fractionation analysis of metals in cell cytoplasm. Pure Appl Chem 80:2595–2608

Ho K-S, Chan W-T (2010) Time-resolved ICP-MS measurement for single-cell analysis and on-line cytometry. J Anal At Spectrom 25:1114–1122

Isaure M-P, Huguet S, Meyer C, Castillo-michel H, Testemale D, Vantelon D, Saumitou-laprade P, Verbruggen N, Sarret G (2015) Evidence of various mechanisms of Cd sequestration in the hyperaccumulator Arabidopsis halleri, the non-accumulator Arabidopsis lyrata , and their progenies by combined synchrotron-based techniques. J Exp Bot 66:3201–3214

Isaure M-P, Leyh B, Salomé M, Krauss G-J, Schaumlöffel D, Dobritzsch D (2017) The aquatic hyphomycete Heliscus lugdunensis protects its hyphae tip cells from cadmium: a micro X-ray fluorescence and X-ray absorption near edge structure spectroscopy study. Spectrochim Acta Part B At Spectrosc 137:85–92

Ishihara Y, Aida M, Nomura A, Miyahara H, Hokura A, Okino A (2015) Development of Desolvation system for single-cell analysis using droplet injection inductively coupled plasma atomic emission spectroscopy. Anal Sci 31:781–785

Laborda F, Bolea E, Jiménez-Lamana J (2014) Single particle inductively coupled plasma mass spectrometry: a powerful tool for nanoanalysis. Anal Chem 86:2270–2278

Leonardo T, Farhi E, Boisson A, Vial J, Cloetens P, Bohic S (2014) Determination of elemental distribution in green micro-algae using synchrotron radiation nano and quantitative imaging of silver and cobalt. Metallomics 6:316–329

Li F, Armstrong DW, Houk RS (2005) Behavior of bacteria in the inductively coupled plasma: atomization and production of atomic ions for mass spectrometry. Anal Chem 77:1407–1413

Malherbe J, Penen F, Isaure MP, Frank J, Hause G, Dobritzsch D, Gontier E, Horréard F, Hillion F, Schaumlöffel D (2016) A new radio frequency plasma oxygen primary ion source on Nano secondary ion mass spectrometry for improved lateral resolution and detection of electropositive elements at single cell level. Anal Chem 88:7130–7136

Managh AJ, Edwards SL, Bushell A, Wood KJ, Geissler EK, Hutchinson JA, Hutchinson RW, Reid HJ, Sharp BL (2013) Single cell tracking of gadolinium labeled CD4+ T cells by laser ablation inductively coupled plasma mass spectrometry. Anal Chem 85:10627–10634

Maret W (2016) The metals in the biological periodic system of the elements: concepts and conjectures. Int J Mol Sci 17:1–8

Mathieu E, Lai B, Chain F, Langella P, Bachelet M, Masliah J, Seksik P, Policar C (2017) A cell-penetrant manganese superoxide dismutase (MnSOD) mimic is able to complement MnSOD and exerts an Antiinflammatory effect on cellular and animal models of inflammatory bowel diseases. Inorg Chem 56:2545–2555

McRae R, Lai B, Fahrni CJ (2013) Subcellular redistribution and mitotic inheritance of transition metals in proliferating mouse fibroblast cells. Metallomics 5:52–61

Miyashita S, Groombridge AS, Fujii S, Takatsu A, Chiba K, Inagaki K (2014a) Time-resolved ICP-MS measurement: a new method for elemental and multiparametric analysis of single cells. Anal Sci 30:219–224

Miyashita S, Groombridge AS, Fujii S, Minoda A, Takatsu A, Hioki A, Chiba K, Inagaki K (2014b) Highly efficient single-cell analysis of microbial cells by time-resolved inductively coupled plasma mass spectrometry. J Anal At Spectrom 29:1598–1606

Miyashita S, Fujii S, Shigeta K, Inagaki K (2017) Single cell analysis by using ICP-MS. In: Ogra Y, Hirata T (eds) Metallomics: recent analytical techniques and applications. Springer, Berlin, pp 107–124

Mueller L, Traub H, Jakubowski N, Drescher D, Baranov VI, Kneipp J (2014) Trends in single-cell analysis by use of ICP-MS. Anal Bioanal Chem 406:6963–6977

Murray KK, Seneviratne CA, Ghorai S (2016) High resolution laser mass spectrometry bioimaging. Methods 104:118–126

Nomizu T, Nakashima H, Hotta Y, Tanaka T, Kawaguchi H (1992) Simultaneous measurement of the elemental content and size of airborne particles by inductively coupled plasma emission spectrometry combined with the light-scattering method. Anal Sci 8:527–531

Nomizu T, Kaneco S, Tanaka T, Yamamoto T, Kawaguchi H (1993) Determination of Femto-gram amounts of zinc and lead in individual airborne particles by inductively coupled plasma mass spectrometry with direct air-sample introduction. Anal Sci 9:843–846

Nomizu T, Kaneco S, Tanaka T, Ito D, Kawaguchi H, Vallee BT (1994) Determination of calcium content in individual biological cells by inductively coupled plasma atomic emission spectrometry. Anal Chem 66:3000–3004

Nuñez J, Renslow R, Cliff JB, Anderton CR (2018) NanoSIMS for biological applications: current practices and analyses. Biointerphases 13:03B301

Passarelli MK, Ewing AG (2013) Single-cell imaging mass spectrometry. Curr Opin Chem Biol 17:854–859

Penen F, Isaure MP, Dobritzsch D, Bertalan I, Castillo-Michel H, Proux O, Gontier E, Le Coustumer P, Schaumlöffel D (2017) Pools of cadmium in Chlamydomonas reinhardtii revealed by chemical imaging and XAS spectroscopy. Metallomics 9:910–923

Pett-Ridge J, Weber PK (2012) NanoSIP: NanoSIMS applications for microbial biology. In: Navid A (ed) Microbial systems biology. Springer, Berlin, pp 375–408

Qin Z, Caruso JA, Lai B, Matusch A, Becker JS (2011) Trace metal imaging with high spatial resolution: applications in biomedicine. Metallomics 3:28–37

Roschzttardtz H, Grillet L, Isaure M, Conéjéro G, Ortega R, Curie C, Mari S (2011) Plant cell nucleolus as a hot spot for iron. J Biol Chem 286:27863–27866

Roudeau S, Carmona A, Perrin L, Ortega R (2014) Correlative organelle fluorescence microscopy and synchrotron X-ray chemical element imaging in single cells. Anal Bioanal Chem 406:6979–6991

Rubakhin SS, Romanova EV, Nemes P, Sweedler JV (2011) Profiling metabolites and peptides in single cells. Nat Methods 8:S20–S29

Schaumlöffel D, Hutchinson R, Malherbe J, Le Coustumer P, Gontier E, Isaure M-P (2016) Novel methods for bioimaging including LA-ICPMS, NanoSIMS, TEM/X-EDS, SXRF. In: Michalke B (ed) Metallomics: analytical techniques and speciation methods. Wiley-VCH, Weinheim, pp 83–116

Schmid A, Kortmann H, Dittrich PS, Blank LM (2010) Chemical and biological single cell analysis. Curr Opin Biotechnol 21:12–20

Schober Y, Guenther S, Spengler B, Römpp A (2012) Single cell matrix-assisted laser desorption/ionization mass spectrometry imaging. Anal Chem 84:6293–6297

Shigeta K, Traub H, Panne U, Okino A, Rottmann L, Jakubowski N (2013a) Application of a micro-droplet generator for an ICP-sector field mass spectrometer – optimization and analytical characterization. J Anal At Spectrom 28:646–656

Shigeta K, Koellensperger G, Rampler E, Traub H, Rottmann L, Panne U, Okino A, Jakubowski N (2013b) Sample introduction of single selenized yeast cells (Saccharomyces cerevisiae) by micro droplet generation into an ICP-sector field mass spectrometer for label-free detection of trace elements. J Anal At Spectrom 28:637–645

Slaveykova VI, Guignard C, Eybe T, Migeon HN, Hoffmann L (2009) Dynamic NanoSIMS ion imaging of unicellular freshwater algae exposed to copper. Anal Bioanal Chem 393:583–589

Smart KE, Smith JAC, Kilburn MR, Martin BGH, Hawes C, Grovenor CRM (2010) High-resolution elemental localization in vacuolate plant cells by nanoscale secondary ion mass spectrometry. Plant J 63:870–879

Storms HA, Brown KF, Stein JD (1977) Evaluation of a cesium positive ion source for secondary ion mass spectrometry. Anal Chem 49:2023–2030

Szyrwiel L, Shimura M, Shirataki J, Matsuyama S, Matsunaga A, Setner B, Szewczuk Z, Yamauchi K, Chavatte L (2015) A novel branched TAT 47–57 peptide for selective Ni 2+ introduction into the human fibrosarcoma cell nucleus. Metallomics 7:1155–1162

Tanner SD, Bandura DR, Ornatsky O, Baranov VI, Nitz M, Winnik MA (2008) Flow cytometer with mass spectrometer detection for massively multiplexed single-cell biomarker assay. Pure Appl Chem 80:2627–2641

Tsang CN, Ho KS, Sun H, Chan WT (2011) Tracking bismuth antiulcer drug uptake in single helicobacter pylori cells. J Am Chem Soc 133:7355–7357

Týčová A, Ledvina V, Klepárník K (2017) Recent advances in CE-MS coupling: instrumentation, methodology, and applications. Electrophoresis 38:115–133

Umemura T, Matsui Y, Sinnosuke S, Fukai T, Fujimori E, Kumata H, Aoki M (2017) Comprehensive element analysis of prokaryotic and eukaryotic cells as well as organelles by ICP-MS. In: Ogra Y, Hirata T (eds) Metallomics: recent analytical techniques and applications. Springer, Berlin, pp 219–237

Van Malderen SJM, Vergucht E, De Rijcke M, Janssen C, Vincze L, Vanhaecke F (2016a) Quantitative determination and subcellular imaging of cu in single cells via laser ablation-ICP-mass spectrometry using high-density microarray gelatin standards. Anal Chem 88:5783–5789

Van Malderen SJM, Managh AJ, Sharp BL, Vanhaecke F (2016b) Recent developments in the design of rapid response cells for laser ablation-inductively coupled plasma-mass spectrometry and their impact on bioimaging applications. J Anal At Spectrom 31:423–439

Verboket PE, Borovinskaya O, Meyer N, Günther D, Dittrich PS (2014) A new microfluidics-based droplet dispenser for ICPMS. Anal Chem 86:6012–6018

Vergucht E, Brans T, Beunis F, Garrevoet J, De Rijcke M, Bauters S, Deruytter D, Vandegehuchte M, Van Nieuwenhove I, Janssen C, Burghammer M, Vincze L (2015) In vivo X-ray elemental imaging of single cell model organisms manipulated by laser-based optical tweezers. Sci Rep 5:9049

Wang D, Bodovitz S (2010) Single cell analysis: the new frontier in "omics". Trends Biotechnol 28:281–290

Wang HAO, Grolimund D, Giesen C, Borca CN, Shaw-Stewart JRH, Bodenmiller B, Günther D (2013) Fast chemical imaging at high spatial resolution by laser ablation inductively coupled plasma mass spectrometry. Anal Chem 85:10107–10116

Wang H, Wang B, Wang M, Zheng L, Chen H, Chai Z, Zhao Y, Feng W (2015) Time-resolved ICP-MS analysis of mineral element contents and distribution patterns in single cells. Analyst 140:523–531

Wang H, He M, Chen B, Hu B (2017a) Advances in ICP-MS-based techniques for trace elements and their species analysis in cells. J Anal At Spectrom 32:1650–1659

Wang H, Chen B, He M, Hu B (2017b) A facile droplet-Chip-time-resolved inductively coupled plasma mass spectrometry online system for determination of zinc in single cell. Anal Chem 89:4931–4938

Wedlock LE, Kilburn MR, Cliff JB, Filgueira L, Saunders M, Berners-Price SJ (2011) Visualising gold inside tumour cells following treatment with an antitumour Au(I) complex. Metallomics 3:917–925

Wolfe-Simon F, Switzer Blum J, Kulp TR, Gordon GW, Hoeft SE, Pett-Ridge J, Stolz JF, Webb SM, Weber PK, Davies PCW, Anbar AD, Oremland RS, Hille R, Lane TW, Morel FM, Wolfe-Simon F, Davies PCW, Anbar AD, Rosen BP, Baer CD, Edwards JO, Rieger PH, Oremland RS, Stolz JF, Hollibaugh JT, Blum JS, Bindi AB, Buzzelli J, Stolz JF, Oremland RS, Takeuchi M, Makino W, Cotner J, Sterner R, Elser J, Mandelstam J, Smith PG, Pickering IJ, Holbrook S, Dickerson R, Kim SH, Oremland RS, Stolz JF, Quillaguaman J, Delgado O, Mattiasson

B, Hatti-Kaul R (2011) A bacterium that can grow by using arsenic instead of phosphorus. Science 332:1163–1166

Zavalin A, Todd EM, Rawhouser PD, Yang J, Norris JL, Caprioli RM (2012) Direct imaging of single cells and tissue at sub-cellular spatial resolution using transmission geometry MALDI MS. J Mass Spectrom 47:1473–1481

Zhao F, Moore KL, Lombi E, Zhu Y (2014) Imaging element distribution and speciation in plant cells. Trends Plant Sci 19:183–192

Zheng L-N, Wang M, Wang B, Chen H-Q, Ouyang H, Zhao Y-L, Chai Z-F, Feng W-Y (2013) Determination of quantum dots in single cells by inductively coupled plasma mass spectrometry. Talanta 116:782–787

Zheng L-N, Wang M, Zhao L-C, Sun B-Y, Wang B, Chen H-Q, Zhao Y-L, Chai Z-F, Feng W-Y (2015) Quantitative analysis of Gd@C82(OH)22 and cisplatin uptake in single cells by inductively coupled plasma mass spectrometry. Anal Bioanal Chem 407:2383–2391